INT. J. GEOGRAPHICAL INFORMATION SCIENCE, 2002
VOL. 16, NO. 5, 475–501

Taylor & Francis
Taylor & Francis Group

Research Article

Errors of signal processing in digital terrain modelling

IGOR V. FLORINSKY

Department of Soil Science, University of Manitoba, 362 Ellis Bldg, Winnipeg, Manitoba, R3T 2N2, Canada and Institute of Mathematical Problems of Biology, Russian Academy of Sciences, Pushchino, Moscow Region, 142292, Russia; e-mail: florinskyi@em.agr.ca

(*Submitted 19 July 2000; accepted 20 July 2001*)

Abstract. We present new interpretation of three classes of errors in digital terrain models (DTMs) which can be sources of artefacts in DTM-based studies: (*a*) errors in interpolation of digital elevation models (DEMs) caused by the Gibbs phenomenon; (*b*) errors in DTM derivation from DEMs with 'enhanced' resolution due to noise increase after DEM differentiation; (*c*) errors in DTM derivation caused by displacement of a DEM grid. Explanation of artefact roots and ways to avoid them are carried out in the context of the theory of signal processing. The Gibbs phenomenon is a specific behaviour of some functions manifested as over- and undershoots near a jump discontinuity. Any DEM includes jump discontinuities of the elevation, such as escarpments and pronounced errors of DEM generation. There are four main ways to prevent or reduce DEM errors caused by the Gibbs phenomenon: (*a*) decreasing the jump discontinuity before DEM interpolation; (*b*) using interpolation functions which do not generate the Gibbs phenomenon; (*c*) omitting over- and undershoots after DEM interpolation; (*d*) filtering the Gibbs phenomenon. Derivation of topographic variables from DEMs marked by 'enhanced' resolution can lead to artefacts. If a DEM of this kind is interpolated by triangulation-based algorithms, triangular patterns may be revealed on maps of topographic variables. If an 'enhanced' resolution of DEM is achieved by the weighted average methods of interpolation, contour 'traces' may be seen on maps. This is because partial derivatives used to calculate some topographic variables are very responsive to high-frequency components of a DEM. To prevent these errors one should use a regular DEM with a grid space relating to an average distance between points in an irregular DEM. Displacement of a grid of points, wherein elevation values are interpolated or determined, influences the derivation of topographic variables (e.g. map design of horizontal and vertical curvatures). Some patterns break, merge, and change their width and length. Small dots, lines, and particles of big patterns can appear and disappear on maps. These effects should be taken into account in the application of these maps to DTM-based geological studies.

1. Introduction

Digital terrain modelling can be defined as a system of quantitative methods to analyse and model the landsurface and relationships between the topography and geological, hydrological, biological and anthropogenic components of the landscape.

International Journal of Geographical Information Science
ISSN 1365-8816 print/ISSN 1362-3087 online © 2002 Taylor & Francis Ltd
http://www.tandf.co.uk/journals
DOI: 10.1080/13658810210129139

By digital terrain models (DTMs) we mean digital representations of variables describing the topographic surface, namely: digital elevation models (DEMs), digital models of slope gradient (G), aspect (A), horizontal (k_h), vertical (k_v), mean (H) and Gaussian (K) landsurface curvatures (Appendix), specific catchment area, topographic and stream power indices as well as some other topographic attributes (Burrough 1986, Shary 1995). Digital terrain modelling is extensively used in geosciences (Moore *et al.* 1991, Shary *et al.* 1991, Weibel and Heller 1991, Florinsky 1998a, Pike 2000).

A large number of studies have been focused on aspects of the problem of errors in digital terrain modelling, such as types, sources and effects of DTM errors, methods for their recognition, analysis, measurements, mapping and prevention (see details and references in Florinsky 1998a). In particular, much attention has been given to DTM errors as sources of artefacts, such as false landforms (McCullagh 1988, 1998, Wood and Fisher 1993, Robinson 1994, Eklundh and Mårtensson 1995, Hunter and Goodchild 1995, Desmet 1997, Veregin 1997, Wise 1998, Endreny *et al.* 2000). This topic is important because false landforms initiated by DTM errors can lead to geomorphic and geological misinterpretation of DTMs. Also, these artefacts can adversely effect DTM-based hydrological, soil and geomorphic modelling due to propagation of DTM errors (Weibel and Brändli 1995, Desmet 1997, Bates *et al.* 1998, Wise 2000).

From the algorithmic standpoint, digital terrain modelling can be considered as a special case of the more general field of signal processing. Some common mathematical methods and technical principles of this field are employed in digital terrain modelling, such as approximation, discretisation (sampling), interpolation and differentiation (Mitra 1998). Thus some errors of digital terrain modelling have analogues in signal processing. Among them, there are three classes of errors that have not been adequately studied, as applied to digital terrain modelling:

- Errors in DEM interpolation caused by the Gibbs phenomenon;
- Errors in DTM derivation from DEMs with 'enhanced' resolution due to noise increase after DEM differentiation;
- Errors in DTM derivation caused by the displacement of DEM grids.

These errors create false landforms, so their examination is particularly important for geomorphic and geological applications of digital terrain modelling. The objective of this study is to describe theoretical causes and effects of these three classes of DTM errors, to present examples, and to discuss practical ways to prevent them in digital terrain modelling.

2. Errors in DEM interpolation caused by the Gibbs phenomenon

2.1. *Problem statement*

The Gibbs phenomenon is a specific behaviour of some functions manifested as over- and undershoots around a jump discontinuity (Hewitt and Hewitt 1980, Jerri 1998). The Gibbs phenomenon is typical for the Fourier series, orthogonal polynomials, splines, wavelets, and some other approximation functions (Jerri 1998). It appears in many scientific problems and applications involving digital signal and image processing (Rosenfeld and Kak 1982, Mitra 1998).

For the one-dimensional case, the simplest mathematical illustration of the Gibbs

phenomenon is an approximation of a square wave function (figure 1(*a*))

$$F(x)=\begin{cases}1, & 0<x<\pi\\ 0, & x=0,\ \pm\pi\\ -1, & -\pi<x<0\end{cases} \tag{1}$$

by a trigonometric polynomial of the form

$$f_{2k-1}(x)=\frac{4}{\pi}\sum_{k=1}^{\infty}\frac{\sin(2k-1)x}{2k-1}=\frac{4}{\pi}\left(\sin x+\frac{\sin 3x}{3}+\ldots+\frac{\sin(2k-1)x}{2k-1}\right) \tag{2}$$

The polynomial (equation (2)) converges uniformly to the square wave function (equation (1)) except at points $x=0,\ \pm\pi$ which are points of discontinuity of $F(x)$. This means that as k increases, graphs of the partial sums $f_{2k-1}(x)$ adjoin arbitrarily closely the lines $F(x)=\pm 1$ except near the points $x=0,\ \pm\pi$ (figures 1(b–e)). This defect of convergence manifests itself as over- and undershoots around the points $x=0,\ \pm\pi$. It is important that as k increases, a vertical size of these over- and undershoots does not decrease (figures 1(*b–e*)). It is equal to 17.9% of half the jump size or 8.95% of the jump size. As $k\to\infty$, an ultimate geometrical image of curves $f_{2k-1}(x)$ is a jogged line including extended vertical legs as big as 8.95% of the jump size (figure 1(*f*)) (Fikhtengolts 1966). Increasing k, it is possible to reduce the horizontal extension of the Gibbs phenomenon only (figure 1).

In the Gibbs phenomenon, over- and undershoot size depends on the size of the jump discontinuity and a sort of function. In the classical case of the Fourier series,

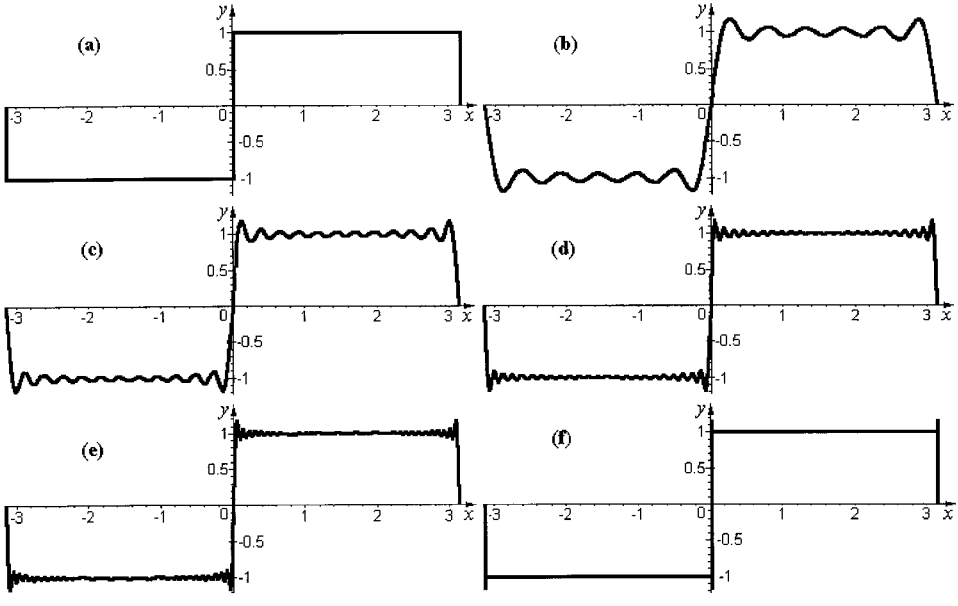

Figure 1. Approximation of the square wave function by the trigonometric polynomial: (*a*) square wave function; partial sums: (*b*) $k=6$, (*c*) $k=12$, (*d*) $k=24$, (*e*) $k=36$, (*f*) $k\to\infty$.

the over- and undershoot size is equal to 8.95% of the jump size (Jerri 1998). Fikhtengolts (1966) established that the Gibbs phenomenon takes place for any piecewise-smooth function, such as splines; the over- and undershoot size is 8.95% of the jump size for a spline of the order $k \to \infty$. Richards (1991) demonstrated that the over- and undershoot size increases when the order of a spline decreases. For example, it is 9.49% and 13.39% of the jump size for $k = 8$ and $k = 2$, correspondingly; the greater the jump, the greater the over- and undershoots.

Since splines and other approximation functions are widely used for DEM interpolation (Watson 1992), knowledge of the properties of the Gibbs phenomenon becomes necessary to provide correct digital terrain modelling, particularly to choose an appropriate method of interpolation to reduce or eliminate over- and undershoots. Practically, any DEM includes many jump discontinuities of the elevation function wherein the Gibbs phenomenon can arise after interpolation. These are areas marked by sharp changes of elevation (or steep gradient), such as terraces, escarpments, abrupt slopes, peaks, pits, etc. Jump discontinuities of the elevation can also occur near pronounced systematic and random errors of DEM generation, for example, near an abrupt linear step in elevations resulting from processing an orthophoto as separate patches and subsequently joining them to assemble a DEM (Hunter and Goodchild 1995), or near a point with a false elevation of 100 m within an area with average altitude of 10 m.

After interpolation, DEM errors caused by the Gibbs phenomenon can arise near these jump discontinuities. For instance, the two artificial 'landforms' may appear near a steep scarp: a 'bank' (an overshoot) along the escarp edge, and a 'ditch' (an undershoot) along the escarp foot. The relative height of the 'bank' as well as relative depth of the 'ditch' for a 50 m scarp can be about 4.5 m (8.95% of 50 m) if the interpolation is carried out with high order splines. Artificial closed 'banks' (overshoots) and 'ditches' (undershoots) may arise around isolated pits and peaks, correspondingly.

DEM interpolation has been commonly used in the past four decades, so DTM researchers have noted over- and undershoots near steep gradients in interpolated DEMs as well as trying to solve this problem (§ 2.3) (Akima 1974, McCullagh 1981, Nielson and Franke 1984, Mitášová and Mitáš 1993). Unfortunately, these authors did not recognise over- and undershoots as a manifestation of the Gibbs phenomenon. Understanding the cause, however, leads to efficient and correct handling of the offer.

In the next section, we discuss properties of the Gibbs phenomenon and ways to prevent it, as applied to digital terrain modelling.

2.2. *Materials and methods*

A DEM of an imaginary site was manually compiled. The site measures 7 m × 7 m. The square-gridded DEM consists of 64 points. The site includes two jump discontinuities: (*a*) a scarp with a difference in elevations of about 26 m and a planimetric distance between edge and foot of about 1 m, and (*b*) an false elevation of −100 m within an area marked by an average elevation of −4 m (figure 2(*a*)).

Two DEMs with a grid size (w) of 0.03 m were derived from the initial DEM by the Delaunay triangulation and a linear interpolation (figure 2(*b*)) as well as the Delaunay triangulation and a piecewise quadric polynomial interpolation with

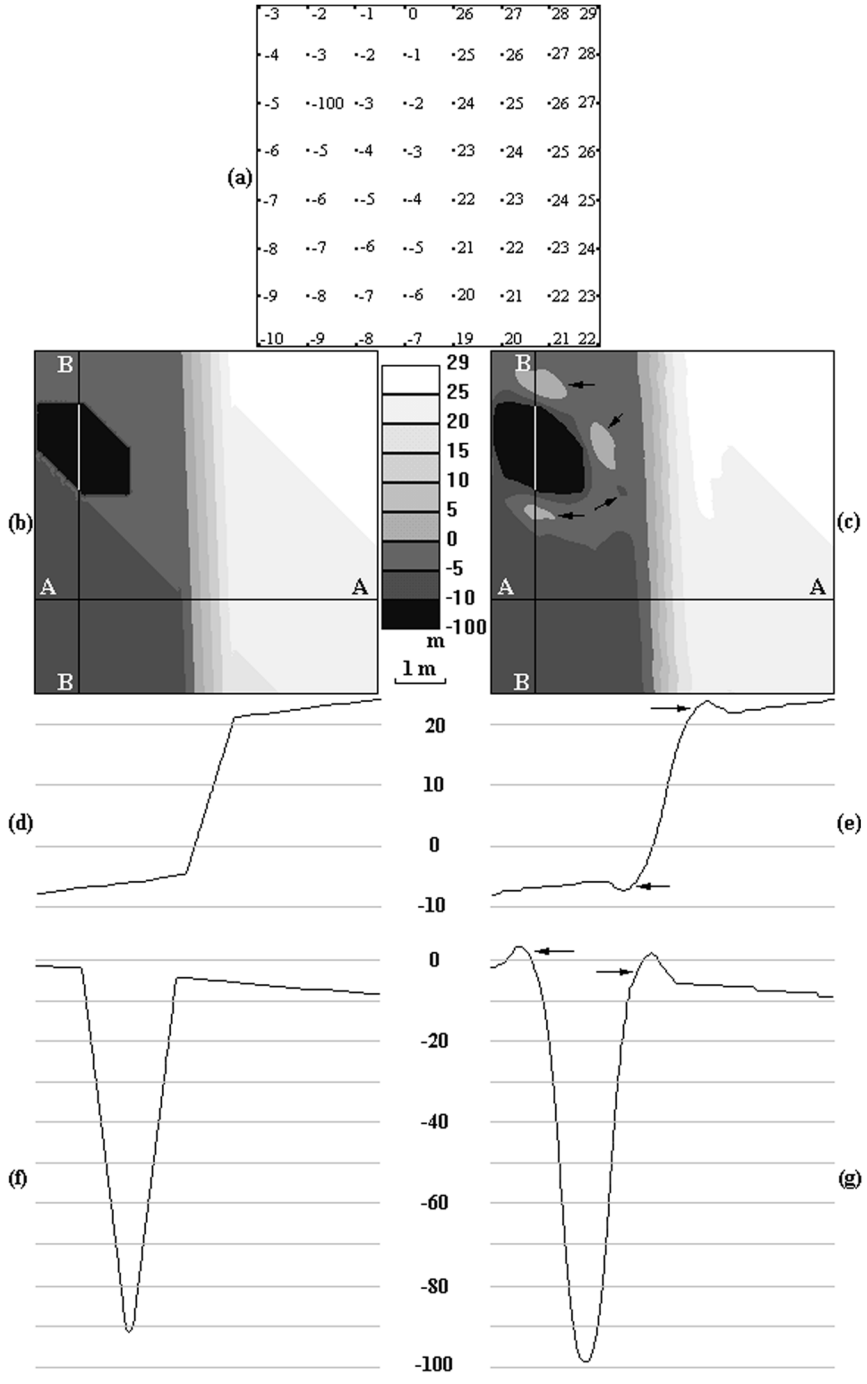

Figure 2. The Gibbs phenomenon in DEM interpolation: (*a*) distribution of points with measured elevations; (*b*) elevation map produced by the Delaunay triangulation with a linear interpolation; (*c*) elevation map produced by the Delaunay triangulation with a smooth interpolation, A–A and B–B are lines of cross-sections through areas with jump discontinuities; (*d*) cross-section A–A for the DEM produced with a linear interpolation; (*e*) cross-section A–A for the DEM produced with a smooth interpolation; (*f*) cross-section B–B for the DEM produced with a linear interpolation; (*g*) cross-section B–B for the DEM produced a smooth interpolation. Arrows indicate the Gibbs phenomenon.

matching derivatives along triangle edges (figure 2(*c*)) (Watson 1992). Notice that there is the degenerate condition of the Delaunay triangulation for any square gridded lattice. This is because each four adjacent points of the lattice have two possible triangulations satisfying the empty circle criterion. This well-known problem can be prevented easily by inserting a minor random displacement into each datum (Watson 1992).

Cross-sections A–A and B–B were constructed through the jump discontinuities (figures 2(*b*) and (*c*)).

2.3. *Results and discussion*

On an elevation map produced by the Delaunay triangulation with a smooth interpolation, one can see three marks ('knolls') of the Gibbs phenomenon around the false elevation (figure 2(*c*)). With the exception of a small 'pit', the elevation map does not demonstrate marks of the Gibbs phenomenon along the scarp due to the large contour interval (figure 2(*c*)). At the same time, there are no marks of the Gibbs phenomenon on an elevation map produced by the Delaunay triangulation with a linear interpolation (figure 2(*b*)).

A cross-section A–A without features of the Gibbs phenomenon is presented on figure 2(*d*). It relates to the DEM produced by the Delaunay triangulation with a linear interpolation (figure 2(*b*)). At the same time, there are artefacts of the Gibbs phenomenon on a cross-section A–A corresponding to the DEM produced by the Delaunay triangulation with a smooth interpolation (figure 2(*c*)). These are over- and undershoots to the left and to the right of the jump discontinuity (figure 2(*e*)). So, two 'landforms' arose due to the Gibbs phenomenon after a smooth interpolation: the 'bank' is along the edge, and the 'ditch' is along the foot.

A cross-section B–B without marks of the Gibbs phenomenon is presented on figure 2(*f*). It relates to the DEM produced by the Delaunay triangulation with a linear interpolation (figure 2(*b*)). At the same time, there are two marks of the Gibbs phenomenon on a cross-section B–B corresponding to the DEM produced by the Delaunay triangulation with a smooth interpolation (figure 2(*c*)). These overshoots are part of the 'bank' around the 'hole' connected with the false elevation of -100 m (figure 2(*g*)).

The results (figure 2) demonstrate that the Gibbs phenomenon can arise after a smooth interpolation rather than a linear one.

DEM errors caused by the Gibbs phenomenon can propagate through the processing and produce new errors in DTMs derived from a DEM. Errors in digital models of the local topographic attributes (Appendix) can arise around areas marked by the Gibbs phenomenon. In this case, a manifestation of the Gibbs phenomenon may be increased since the derivation of these DTMs is carried out with calculation of the first and second derivatives of the elevation function (Appendix). It is well known that differentiation of a signal can increase noise (§ 3.1). Errors in digital models of specific catchment area and a topographic and stream power indices can arise in each point located downslope from the Gibbs phenomenon rather than near jump discontinuities only. This is because these topographic variables accumulate their values downslope. As vertical errors adversely affect determination of flow-path direction (Veregin 1997), the Gibbs phenomenon can disturb a design of drainage network maps.

Since the Gibbs phenomenon takes place near a jump discontinuity after DEM interpolation by some functions, and the size of over- and undershoots is proportional

to the jump, there are four main ways to prevent or reduce DEM errors caused by the Gibbs phenomenon:

1. Decreasing the jump discontinuity before DEM interpolation.
2. Using interpolation functions that do not generate the Gibbs phenomenon.
3. Omitting over- and undershoots after DEM interpolation.
4. Filtering the Gibbs phenomenon.

The first way can be carried out by more detailed description of the jump inserting additional points into an irregular DEM within the area with a jump discontinuity. This should be done before interpolation of the irregular DEM into a regular one. For example, the irregular DEM includes a scarp described by two sets of points along its edge and foot. To reduce the jump discontinuity, it would be rational to insert at least one additional set of points along a mid-slope of the escarp. This sort of densification can decrease over- and undershoots or may hold an interpolation function in position without over- and undershoots, as jump magnitudes are decreased and the function passes through (or approximates to) additional points. Since the densification is carried out before the interpolation, it neither violates the regular uniform raster nor leads to an overall densification of the grid of the regular DEM. A 'drawback' of this way is the necessity of careful control of the generation of the irregular DEM including a choice of a proper distribution of nodes for the DEM network. However, this is a common problem of DEM derivation.

The second option may be performed using algorithms of linear interpolation as we demonstrated above. These methods are certainly free of the Gibbs phenomenon, but they may generate discretisation artefacts in the regular DEM if the irregular DEM is widely spaced. Methods of smooth interpolation are commonly used to avoid this problem, but they can generate errors caused by the Gibbs phenomenon. To solve this problem, one may use some smooth interpolation schemes based on splines with tension (Nielson and Franke 1984, Mitášová and Mitáš 1993). These methods do not generate discretisation artefacts because a smooth interpolation is applied. They were developed to protect DEM interpolation from over- and undershoots near jump discontinuities. However, over- and undershoots were not recognized as manifestations of the Gibbs phenomenon in the papers cited (see a review of tension splines in Watson 1992). A drawback of these methods is the necessity of a choice of tension parameters fitting all jump discontinuities of a specific DEM. Generally, this is an interactive and trial procedure. So, to prevent or reduce DEM errors caused by the Gibbs phenomenon, a user can choose a linear or tension spline interpolation scheme depending on data density in the irregular DEM. Besides, it might be possible to use a method based on the Gegenbauer polynomials (Gottlieb and Shu 1997). However, it is questionable whether this method is adapted for digital terrain modelling.

The third way can be realized by techniques of refinement and interactive editing of DEMs (Weibel and Brändli 1995). A drawback of this way is the necessity of a very careful control of the regular DEM generated by interpolation. An operator should search for over- and undershoots near steep terraces, escarpments, abrupt slopes, peaks, pits, etc. To do this correctly, the operator should be well aware of the actual relief of a studied area. Notice that the Gibbs phenomenon can be useful at this step of the DEM editing. This is because it, as a rule, introduces additional 'banks' and 'ditches' around pronounced random and systematic errors of DEM

derivation. These over- and undershoots may assist the operator to find and eliminate these errors.

The fourth option may be carried out with some kind of special filtering procedures, such as the Fejer averaging and the Lanczos local averaging (Jerri 1998). In this case, the Gibbs phenomenon may be eliminated or reduced since these filters smooth edges of jump discontinuities. However, to do this, the exact location of jump discontinuities must be known. Also, it is doubtful if these filtering procedures are adapted for digital terrain modelling and available in GIS- or DTM-compatible software.

All four ways to prevent or reduce DEM errors caused by the Gibbs phenomenon are rather complex and laborious (excluding linear interpolation). The choice of method depends on the user qualification and available tools.

3. Errors in DTM derivation from DEMs with 'enhanced' resolution due to noise increase after DEM differentiation

3.1. *Problem statement*

Discretisation or sampling of a continuous function and its subsequent reconstruction from a discrete function or sampled points by interpolation are typical procedures of digital signal and image processing (Rosenfeld and Kak 1982, Jähne 1991, Mitra 1998). According to the Kotelnikov–Shannon sampling theorem, a one-dimensional continuous bandlimited function $y=f(x)$ with a bandwidth v can be completely determined by a set of samples $f(k\Delta x)$ if the sampling interval, $\Delta x \leqslant 1/2v$, $-\infty \leqslant k \leqslant \infty$ (Benedetto and Ferreira 2000). An extension of the sampling theorem to a two-dimensional case holds that a continuous bandlimited function $z=f(x, y)$ with bandwidths v_x and v_y can be determined by a set of samples $f(k\Delta x, l\Delta y)$ if sampling intervals $\Delta x \leqslant 1/2v_x$ and $\Delta y \leqslant 1/2v_y$, $-\infty \leqslant k, l \leqslant \infty$. In other words, it is possible to reconstruct a continuous function from a discrete one if at least two samples per the shortest wavelength $\lambda_{x,y}$ were collected, $\lambda_{x,y}=1/v_{x,y}$ (Rosenfeld and Kak 1982, Jähne 1991). Practically, to avoid ambiguity in reconstruction of a function due to limitations of the sampling theorem and interpolation effects (e.g., the Gibbs phenomenon–§ 2.1), it is advisable to use a multiplicative factor $n=(2 \div 10)$ to determine sampling intervals $\Delta x \leqslant \tilde{\lambda}_x/2n$ and $\Delta y \leqslant \tilde{\lambda}_y/2n$ (Grigorenko 1998).

DEM generation is a discretisation of a two-dimensional function of the landsurface elevation (Makarovič 1973, 1976, 1977, Mark 1975, Stefanovic *et al.* 1977, Carter 1988). As in the case of any actual signal, the landsurface spectrum is unlimited, so the condition of the sampling theorem is not met (Baker 1982, Robinson 1994, Grigorenko 1998). This is a tractable problem because a user is usually interesting to study landsurface elements with typical sizes not smaller than threshold short wavelengths $\tilde{\lambda}_{x,y}$ (Mark 1975). So, it is possible to consider, in each given case, that the landsurface elevation is bandlimited function with bandwidths $\tilde{v}_{x,y}$.

The sampling theorem, as applied to digital terrain modelling, has three obvious consequences:

1. To keep information on short wavelength features of the landsurface with typical planimetric sizes $\tilde{\lambda}_{x,y}$ in a DEM, one should use sampling intervals $\Delta x \leqslant \tilde{\lambda}_x/2n$ and $\Delta y \leqslant \tilde{\lambda}_y/2n$, or $w \leqslant \tilde{\lambda}_{x,y}/2n$ for square-gridded sampling (Mark 1975). Then a spatial resolution of the DEM corresponds to $\tilde{\lambda}_{x,y}$. This is a resolution limit of the DEM and all DTMs derived from this DEM.

2. Using interpolation, it is impossible to attain a spatial resolution of an interpolated DEM higher than the resolution of the DEM before interpolation. In other words, it is impossible to reconstruct landsurface features with typical sizes less than $\tilde{\lambda}_{x,y}$. A formal DEM resolution may clearly be 'enhanced' by interpolation using $w \ll \Delta x, \Delta y$, but this procedure cannot improve an actual DEM resolution (Stefanovic *et al.* 1977, Horn 1981, Sasowsky *et al.* 1992).
3. DEM features with typical planimetric sizes less than $\tilde{\lambda}_{x,y}$ generated by interpolation should be considered as high-frequency noise caused by properties of an interpolation method.

This high-frequency noise may not be clearly seen in elevation maps derived from DEMs with 'enhanced', or over-detailed resolution. This is because the vertical magnitude of the noise may be too small compared with a contour interval. However, these minor false 'landforms' may be dramatically increased in subsequent processing of the DEM, such as derivation of topographic variables using differentiation procedures (Appendix).

It is common knowledge of signal and image processing that differentiation of a signal increases noise manifestation in a derivative (Baker 1982, Rosenfeld and Kak 1982, Jähne 1991). Sometimes, the noise may not manifest itself clearly in the signal, however it may be accented in the derivative. So, differentiation can impair the signal-to-noise ratio. Generally, the noise can be marked by a relatively large derivative compared to the signal since the noise is less 'smooth' than the signal, and can fluctuate more randomly than the signal.

The higher the order of the derivative the higher the noise manifestation. The following example can clarify this for the one-dimensional case (figure 3). For an edge in the signal, the first derivative has one extremum (a peak or a pit), while the second derivative has two extrema (a peak and a pit). Also, for a peak or a pit in the signal, the first derivative has two extrema (a peak and a pit), while the second derivative has three extrema (a peak surrounded by two pits or a pit surrounded by two peaks) (figure 3).

Derivation of local topographic variables from DEMs is carried out using the

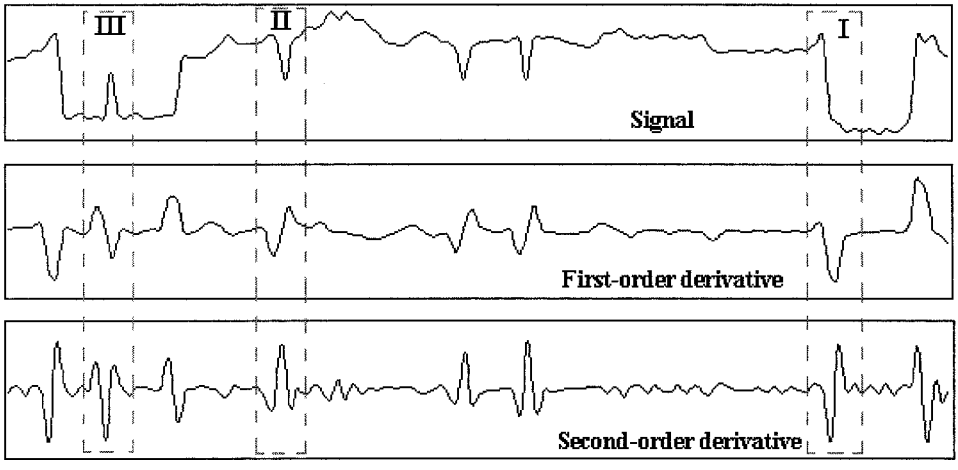

Figure 3. Differentiation of a one-dimensional signal; broken rectangles indicate zones of an edge (I), a pit (II), and a peak (III) of the signal.

first and second partial derivatives of the elevation function (Appendix). As each DEM includes noises (i.e. random and systematic errors), so their propagation with magnification due to differentiation is typical for digital terrain modelling. Some aspects of this kind of DTM error have been discussed previously (Brown and Bara 1994, Giles and Franklin 1996, Desmet 1997, Wise 1998).

It was established that over-detailed DEM interpolation may lead to some problems in subsequent derivation of G due to the roundoff (quantisation) noise in the elevation matrix (Horn 1981, Sasowsky *et al.* 1992). Also, scholars noticed errors typical of DEMs with 'enhanced' resolution, such as terraces, 'traces' of contours and triangular patterns (§3.3) (Batson *et al.* 1975, Wood and Fisher 1993, Eklundh and Mårtensson 1995, Desmet 1997). However, they explained the artefacts observed by problems in interpolation methods, and did not associate them with over-detailed resolution of DEMs.

In the next section, we discuss errors in models of local topographic attributes derived from DEMs with over-detailed resolution due to noise increase after DEM differentiation.

3.2. *Materials and methods*

An irregular DEM of the part of the Crimea and adjacent sea bed was compiled by digitising five 1:300 000 and 1:500 000 scaled topographic maps (Central Board of Geodesy and Cartography 1953, General Headquarters 1986). The area measures 210 km × 132 km. The irregular DEM includes 11936 points (figure 4(*a*)). Different parts of the DEM (e.g. the sea bottom, mountains and plain) are marked by different densities of points. Using the inverse distance weighting interpolation of the irregular DEM (Watson 1992), we produced two regular DEMs with $w = 500$ m (figure 4(*b*)) and $w = 3000$ m.

Application of $w = 500$ m gives an 'enhanced' resolution, since this w value is less than the average distances between points within all parts of the irregular DEM (figure 4(*a*)). The grid size of 3000 m approximately corresponds to average distances between points within the Black and Azov Sea bed and some areas of the Crimean Plain (figure 4(*a*)). The Crimean Mountains can be treated with a smaller grid size, such as 1000 m, but we need to apply one grid size fitting all parts of the DEM.

An irregular DEM of the Severny Gully (Pushchino, Russia) was compiled by a tacheometric survey. The site measures about 58 m × 77 m. The irregular DEM consists of 374 points (figure 5(*a*)). Using the Delaunay triangulation and a piecewise quadric polynomial interpolation with matching derivatives along triangle edges (Watson 1992), we produced two regular DEMs with $w = 0.25$ m (figure 5(*b*)) and $w = 3$ m.

Application of $w = 0.25$ m certainly gives 'enhanced' resolutions since this w value is much less than the average distances between points of the irregular DEM (figure 5(*a*)), whole grid size of 3 m approximately equals the average distances between points of the irregular DEM (figure 5(*a*)).

Digital models of G (figures 4(*c*, *d*) and 5(*c*, *d*)), k_v (figures 4(*e*, *f*)) and k_h (figures 5(*e*) and (*f*)) were derived from the regular DEMs of the Crimea and the Severny Gully by the method of Evans (1980) (Appendix).

To sharpen artefacts on the k_v and k_h maps derived from DEMs with 'enhanced' resolution, we produced 'binary maps' of k_v and k_h, that is, we subdivided k_v and k_h values into two intervals with respect to the zero value (figures 4(*e*, *f*) and 5(*e*, *f*).

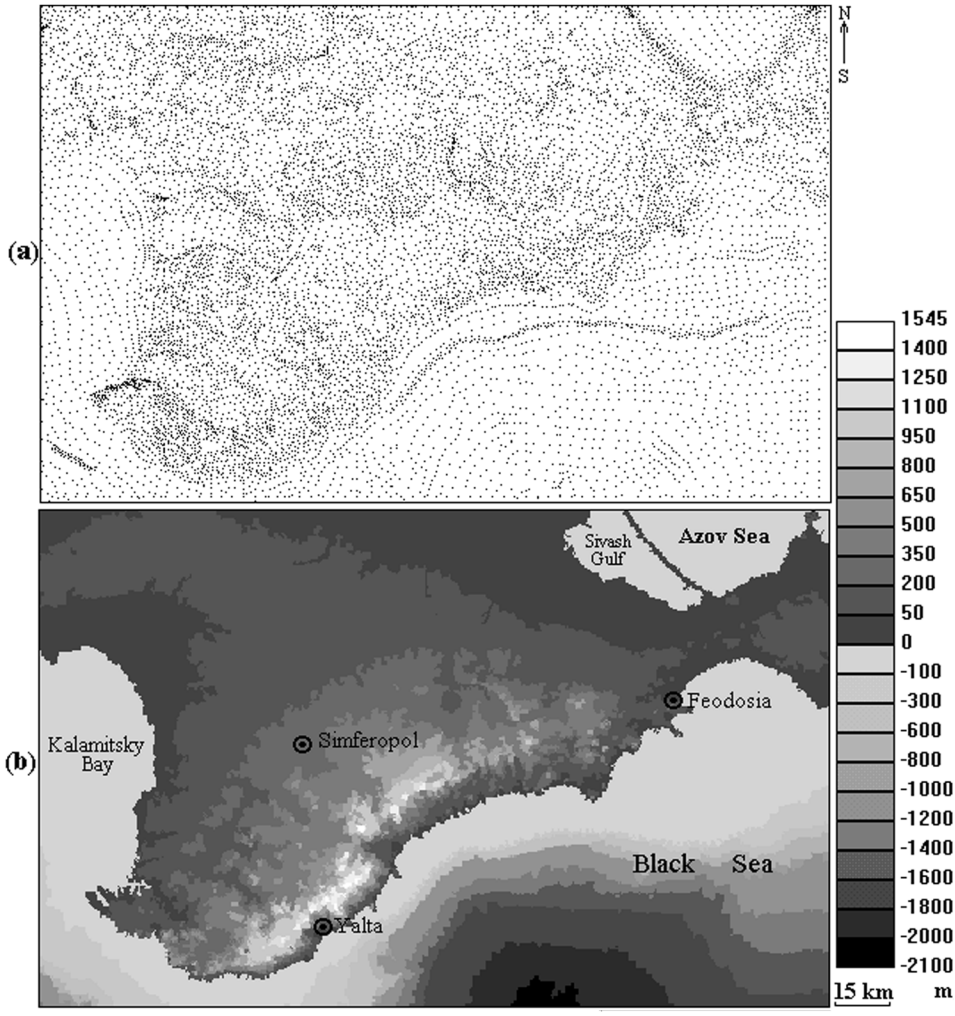

Figure 4. The Crimea and the adjacent sea bottom: (*a*) distribution of points with measured elevations; (*b*) elevation map, $w = 500$ m; (*c*) G map, $w = 500$ m; (*d*) G map, $w = 3000$ m; (*e*) k_v map, $w = 500$ m; (*f*) k_v map, $w = 3000$ m.

3.3. *Results and discussion*

On the G and k_v maps of the Crimea derived from the DEM with $w = 500$ m, one can see 'traces' of contours (i.e. curvilinear artefacts strongly related in form and location to the contours) within the sea bottom and relatively flat areas of the Crimean Plain (figures 4(*c*, *e*)). These maps are unfit for use in any purpose since they display a system of false slender linear 'landforms'. However, G and k_v data derived from the DEM with $w = 3000$ m (figures 4(*d*, *f*)) can be useful in regional-scale geomorphic and geological studies. For example, the k_v map (figure 4(*f*)) was applied successfully to recognise lineaments and faults of the Crimea (Florinsky 1996).

On the G and k_h maps of the Severny Gully derived from the DEM with $w = 0.25$ m, one can see 'marks' of triangulation, such as triangles and other relatively

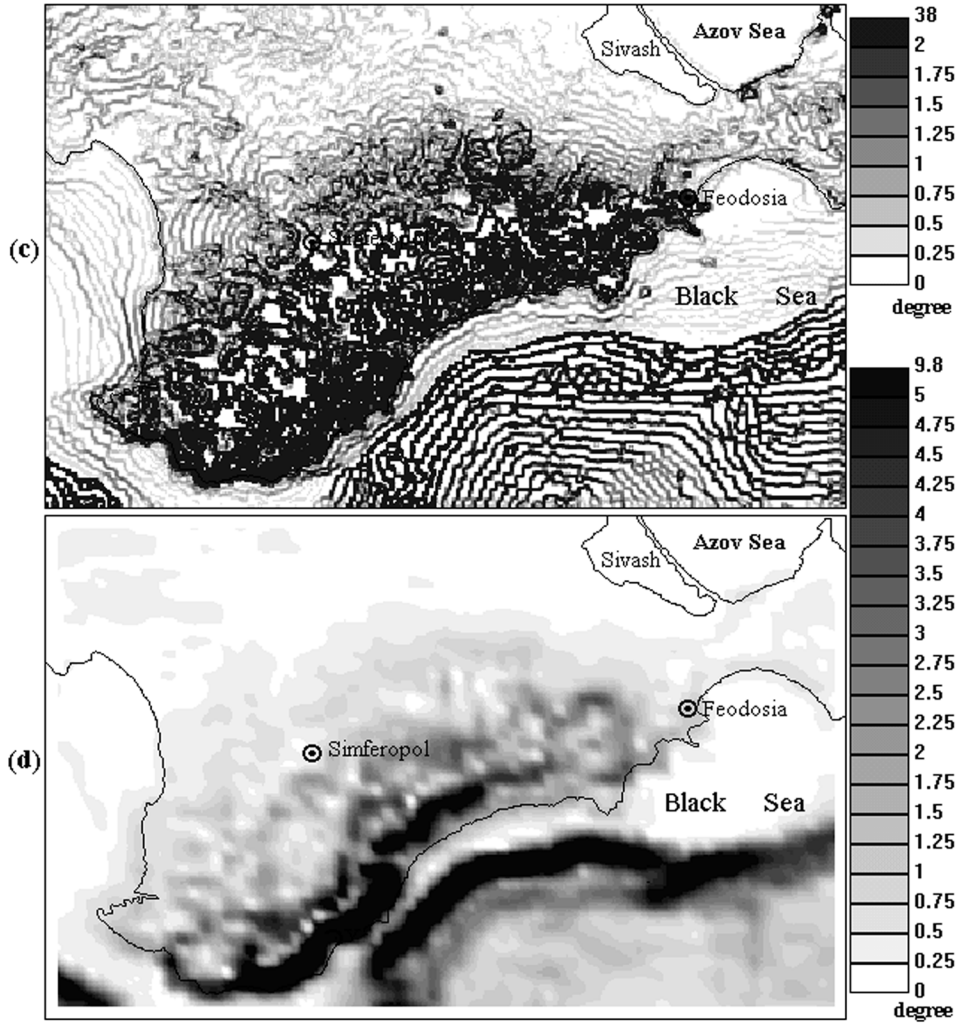

regular features (figures 5(*c*, *e*)). These maps are also unfit for use in any DTM-based application, as they reveal a set of false triangular 'landforms'. At the same time, G and k_h data derived from the DEM with $w = 3$ m (figures 5(*d*, *f*)) were applied successfully to study relationships between soil moisture and topography at a microscale (Florinsky and Kuryakova 2000).

Also, there are significant differences in values of G, k_v and k_h derived from DEMs marked by 'regular' (figures 4(*d*, *f*) and 5(*d*, *f*)) and 'enhanced' resolution (figures 4(*c*, *e*) and 5(*c*, *e*)). This is an expected result since values of topographic attributes depend on DEM resolution (Evans 1980, Chang and Tsai 1991, Carter 1992).

'Traces' of contours (figures 4(*c*, *e*)) are portraits of slender upright artificial 'scarps' of broad flat artificial 'terraces'. 'Scarps' may arise along contours, while 'terraces' can develop between contours in DEM interpolation by the inverse distance weighting method. This is because the method is sensitive to the clustering of points:

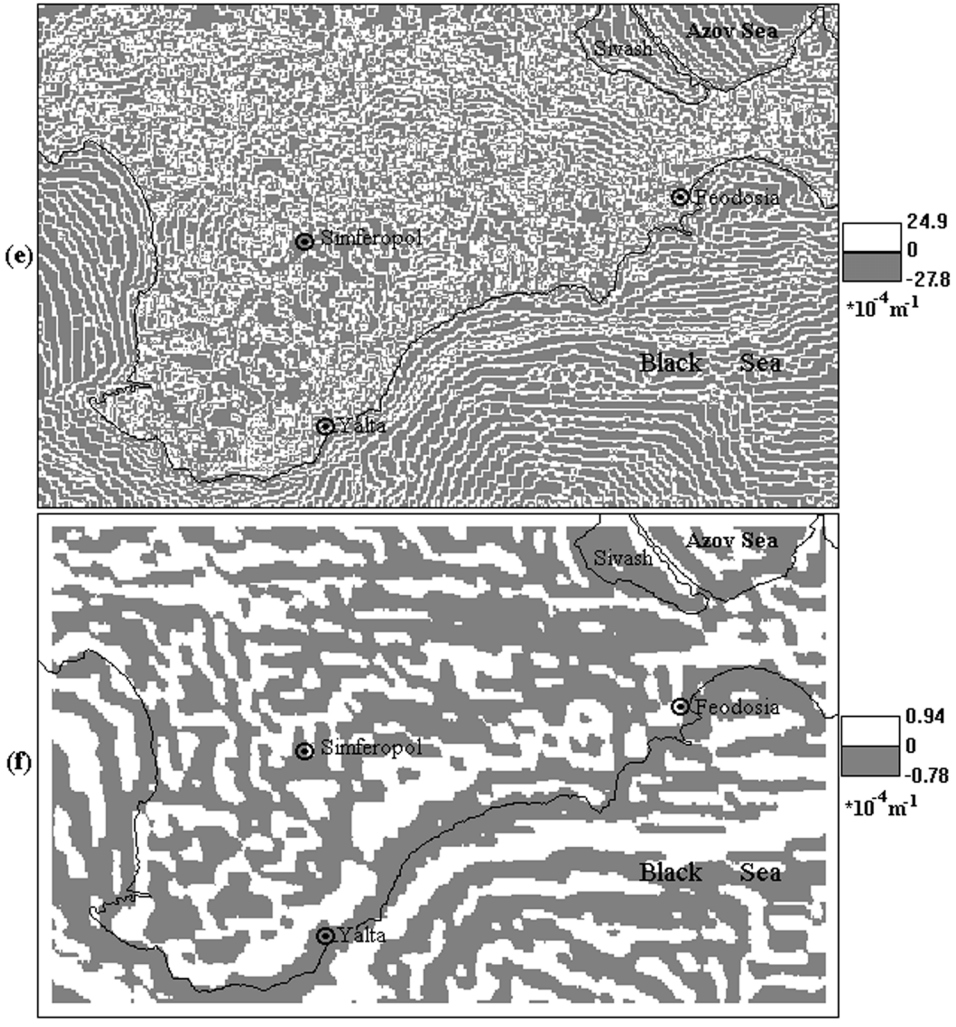

the search of nearest neighbours finds a lot of points along the contours but none across the contours (Wood and Fisher 1993, Eklundh and Mårtensson 1995). As a result, a contour-elevation is assigned to regular DEM points along the contour, while approximately average elevations of two neighbour contours are assigned to regular DEM points between these contours. It has been suggested that the method is not appropriate to interpolate contour-based DEMs (Wood and Fisher 1993, Eklundh and Mårtensson 1995). However, this algorithm imperfection makes itself evident in the case of over-detailed interpolation only. So, this is in fact connected with an evident lack of information between contours at the resolution of $w = 500$ m for the given DEM.

In all probability, triangular artefacts (figures 5(*c*, *e*)) are results of some inaccuracy of the matching derivatives along triangle edges in the piecewise interpolation (Watson 1992). However, this imperfection of the interpolation algorithm makes itself evident in the case of over-detailed interpolation only. So, an actual root of

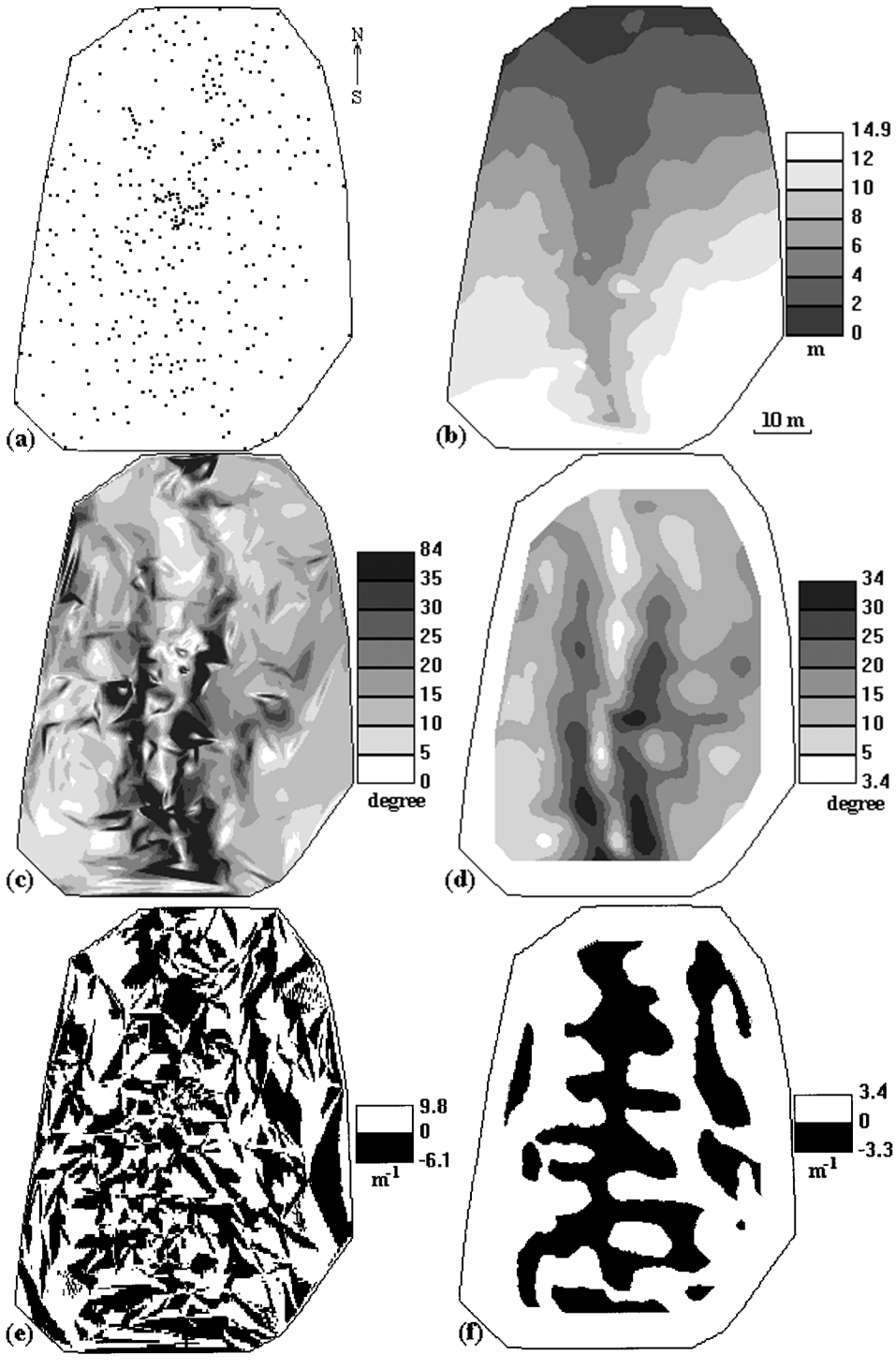

Figure 5. The Severny Gully: (*a*) distribution of points with measured elevations; (*b*) elevation map, $w = 0.25$ m; (*c*) G map, $w = 0.25$ m; (*d*) G map, $w = 3$ m; (*e*) k_h map, $w = 0.25$ m; (*f*) k_h map, $w = 3$ m.

the artefacts is evidently lack of information about elevations between triangulation nodes at the resolution of $w = 0.25$ m for the given DEM.

The inaccuracies discussed lead to relatively minute errors in the regular DEMs with over-detailed resolution. At least, it is impossible to see them on the elevation maps (figures 4(*b*) and 5(*b*)). Therefore, one can ignore these artefacts in some cases: for example, an elevation map derived from a DEM with 'enhanced' resolution can be used for illustration goals. However, these errors are dramatically increased after derivation of G, k_v and k_h as they are calculated by differentiation (Appendix). The same errors may be identified in maps of A, H, K and R since they are also derived from elevation derivatives (Appendix).

There are several ways to avoid these artefacts. First, it has been suggested that more sophisticated and smooth interpolation techniques should be used to prevent formation of terraces in DEMs (Eklundh and Mårtensson 1995), contour traces on G, A, k_v and R maps (Batson *et al.* 1975, Wood and Fisher 1993, Desmet 1997) and triangle patterns on G and A maps (Desmet 1997). Second, Eklundh and Mårtensson (1995) proposed generalizing contours to prevent terraces in DEMs. Third, high frequency filtering and smoothing is applied before differentiation to reduce a level of the high-frequency noise in signal and image processing (Baker 1982, Rosenfeld and Kak 1982, Jähne 1991). Close filtering procedures are used in digital terrain modelling to smooth the high-frequency noise in DTMs derived from DEMs (Horn 1981) or in DEMs before derivation of DTMs (Brown and Bara 1994, Giles and Franklin 1996, Desmet 1997, Wise 1998, 2000).

All these ways may improve results of DEM interpolation and hide a structure of an irregular DEM network. However, this cannot clearly increase an actual resolution of a DEM (conversely, the second option can decrease it). It is incorrect to use DEMs with 'enhanced' resolution for DTM derivation because an over-detailed resolution of a DTM does not relate to actual features of the landsurface kept in a DEM before interpolation. Treating the DTM beyond a resolution limit can lead just to an abstract investigation of a geometry of a matrix of interpolated values $z = f(x, y)$ rather than a geometry of the landsurface.

Common sense guides us to suppose that this is the only appropriate solution of the problem. Since a spatial resolution of an irregular DEM corresponds to $\tilde{\lambda}_{x,y}$, one should use w relating, at least, to $\tilde{\lambda}_{x,y}$ in DEM interpolation, if an interpolated DEM will be then treated for derivation of DTMs. Practically, a value of this w should relate to an average distance between points in the irregular DEM. Other values of w chosen from study task considerations (Florinsky 1996, Florinsky and Kuryakova 2000) should be more than this minimal w. In this case, it is possible to prevent errors in DTM derivation from DEMs with 'enhanced' resolution due to noise-increase after DEM differentiation, as the results demonstrate (figures 4(*d*, *f*), 5(*d*, *f*)). This principle of choosing w for derivation of DTMs from DEMs should be considered as a complementary rule with respect to known requirements for choosing sampling intervals in the generation of irregular DEMs (Makarovič 1973, 1976, 1977, Stefanovic *et al.* 1977, Ayeni 1982, Sasowsky *et al.* 1992).

4. Errors in DTM derivation caused by the displacement of DEM grid

4.1. *Problem statement*

As we have mentioned in §3.1, discretisation of a signal or image and its reconstruction from sampled points are typical procedures of digital signal and image processing (Rosenfeld and Kak 1982, Jähne 1991, Mitra 1998). It is obvious that

somewhat different sets of points can be sampled using different positions of a discretisation grid about the original signal or image. Subsequently, one can produce slightly different reconstructions of the signal or image for different positions of the discretisation grid. As a rule, these minor discretisation errors show as a high-frequency noise, and in most cases one may ignore them. However, they may be increased in secondary products derived from these slightly different signals or images using differentiation (§3.1) (Zlatopolsky 1992).

Discretisation of the two-dimensional function of the landsurface elevation is a key procedure of digital terrain modelling (Makarovič 1973, 1976, 1977, Stefanovic *et al.* 1977). It is well known that the geometry of a DEM grid affects design of maps of topographic variables (Mark 1975, Carter 1988, Robinson 1994, Wilson *et al.* 1998). It is also apparent that slightly different DEMs of the same area can be produced by displacement (in a general case, by rotation) of a grid of points wherein elevation values were interpolated, or determined by a topographic survey or a photogrammetric procedure. We mean that the geometry of an irregular grid or w of a regular grid remains constant, grid position and/or orientation changes only. These DEMs can be marked by minor differences, but all of them may be used to describe the area. Sometimes, grid displacement may improve DEM accuracy: Endreny *et al.* (2000) found that rotation of a SPOT-derived DEM about the axis can improve the root mean square error of the DEM.

The following question arises: what differences could be found in digital models of a topographic attribute derived from a DEM after displacement of a DEM grid? In other words, how does displacement of a DEM grid, wherein elevations are interpolated or determined, influence derivation of topographic characteristics? This problem has only been touched on in previous works. For example, it was established that the rotation of grid points where elevations are determined may lead to 13% odds in values of a topographic volume calculated for earthworks (Sirotkin 1961). Of particular interest is the influence of different positions or orientations of a DEM grid on the DTM-based identification of topographically expressed geological features. Their indicators are linear elements in design of maps of some topographic attributes (Florinsky 1996, 1998b). Tolerance of the identification procedure to DEM grid displacement is not understood.

In the next section, we discuss the influence of displacement of a regular grid of a DEM on design of maps of two topographic variables used in geological studies.

4.2. *Materials and methods*

An area measuring 172 km × 143 km of the interstream area of the Kuma and the Kalaus Rivers (Stavropol Region, Russia) (figure 6(*b*)) was studied. An irregular DEM was compiled by digitising the 1:1 000 000 scaled topographic map (Central Board of Geodesy and Cartography 1968). Elevations were captured by parallel strips at critical points of the landsurface (figure 6(a)). The irregular DEM includes 4459 points.

Using the Delaunay triangulation and a piecewise quadric polynomial interpolation with matching derivatives along triangular edges (Watson 1992), we produced three regular DEMs with $w = 2500$ m. Regular grids of these DEMs have distinct orientations relative to the irregular DEM: rotation angles of the reference axes of the regular grid are 0°, 25°, and 90° in an anti-clockwise direction in relation to the reference axes of the irregular grid (figure 7).

The regular DEM rotated by 90° is different from the regular DEM rotated by

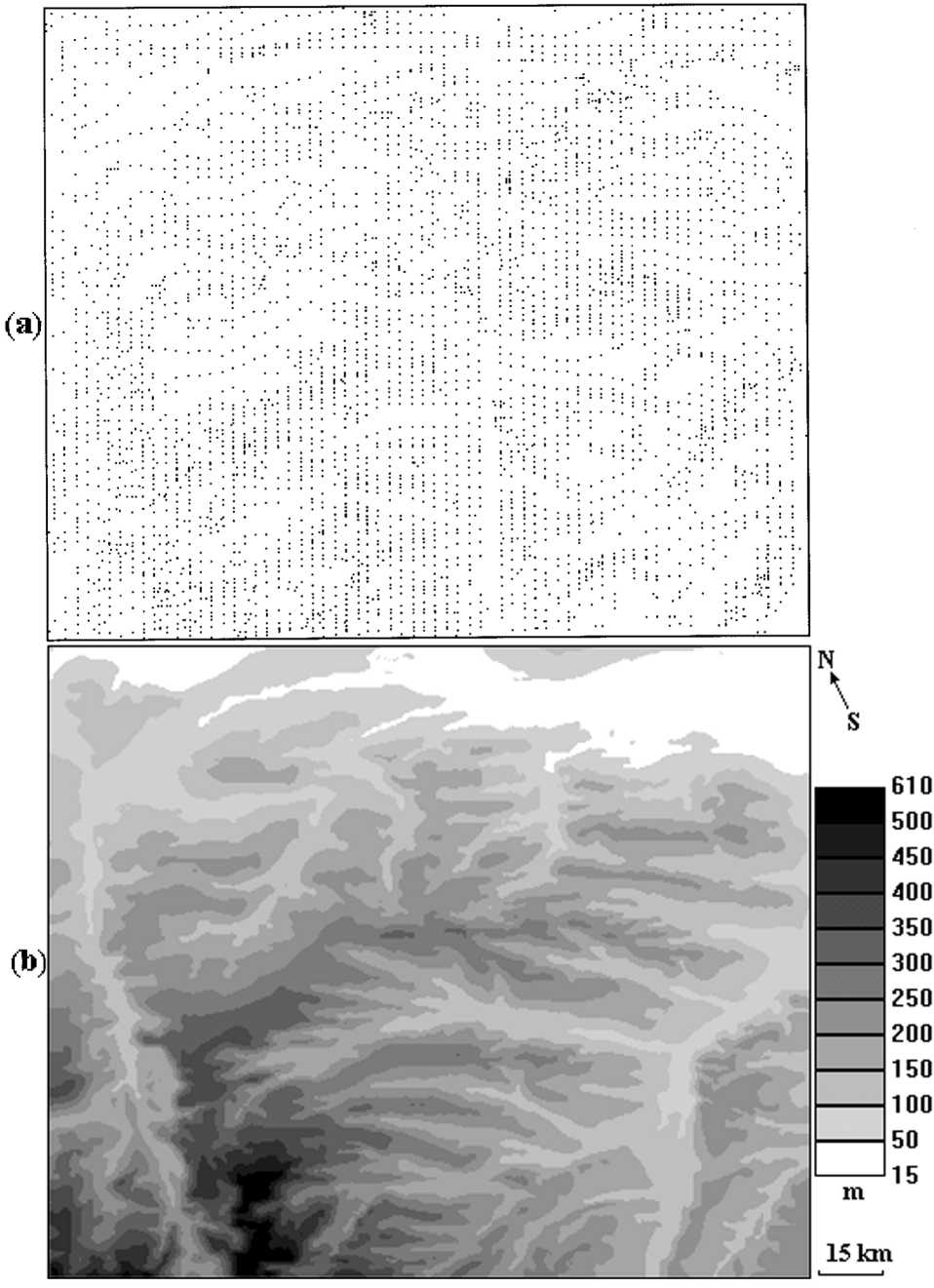

Figure 6. The interstream area of the Kuma and the Kalaus Rivers: (*a*) distribution of points with measured elevations; (*b*) elevation map.

0°, although we used the square-spaced grid. The reason is that the measurements of the irregular DEM (172 km × 143 km) are not multiples of w (2.5 km). As a result of this discrepancy, the measurements of the regular DEMs are 170 km × 142.5 km, since we lost two boundary strips of width 2 km and 0.5 km interpolating the regular

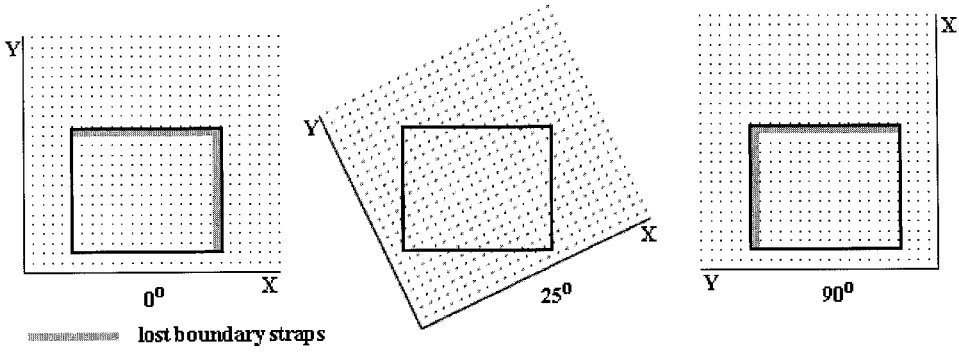

Figure 7. Rotation of the regular grid of the DEM.

DEM from the irregular one. However, the zero of the Cartesian co-ordinate system was displaced after the rotation through 90°: it related to the lower left corner of the area before the rotation, and it moved to the lower right corner after the rotation (figure 7). So, we lost an eastern boundary strap of width 2 km in the DEM rotated by 0°, and a western boundary strap of width 2 km in the DEM rotated by 90° (and a northern boundary strap of width 0.5 km in both DEMs). Therefore, here the rotation of the regular grids through 90° is equivalent to the displacement of the regular grids along the X-axis by 2 km.

Digital models and maps of k_h and k_v (figures 8 and 9) were derived from the three regular DEMs by the method of Evans (1980) (Appendix). We subdivided k_h and k_v values into two intervals with respect to the zero value, because this type of presentation of k_h and k_v data is used for lineament and fault identification (Florinsky 1996, 1998b).

4.3. *Results and discussion*

Visual comparative analysis of the results demonstrates that the DEM rotation leads to identification of slightly different topographic patterns. Although the k_h and k_v maps derived from the variously oriented DEMs have many similarities, they also include a number of distinctions (figures 8 and 9). In particular, some patterns break or merge, and some patterns change their width and length. Most patterns retain their position. However, small dots, narrow lines and small particles of big patterns appear and disappear on maps. Notice that typical sizes of these patterns are less than w. Therefore, they fit into a high-frequency noise (§3.1). Also, there are minor changes in value intervals of k_h and k_v (figures 8 and 9).

These artefacts are manifestations, within certain limits, of DEM discretization errors (§4.1) increased by differentiation used in calculation of k_h and k_v (Appendix, §3.1). This is analogous to effects arising in lineament identification by digital processing of remotely sensed images: parts of linear structures can appear and disappear due to the image rotation in relation to the discretisation grid (Zlatopolsky 1992). It is not possible to prevent these effects completely because digital terrain modelling is a transformation of discrete functions describing the continuum of the topographic surface with a given level of accuracy (§3.1).

It is possible to observe that some patterns slightly alter their form and orientation according to the rotation of the regular grid in the central part of the studied area (figures 8 and 9). This is influenced by the discrete geometry of the square-spaced

DTM grid on a map design: the bigger w of the grid, the stronger manifestation of the raster, and the more significant changes may be found in a map design after displacement of the grid. We may suppose that k_h is more sensitive to the discrete geometry of the grid than k_v, since changes in pattern orientation on the k_v map are less than on the k_h map (figures 8(*b*) and 9(*b*)). However, most of patterns retain their orientation after rotation (figures 8 and 9). So, although some patterns of these maps are affected by the displacement of the grid, the effect is not dramatic.

However, changes in a map after rotation of a regular DEM grid may be more composite. In addition to discretisation errors and the influence of the discrete geometry of the grid, these changes may be caused by possible anisotropy of operators for derivation of topographic variables as well as moral anisotropy of interpolation. It is hard to separate the effects of these causes, especially as anisotropy of operators of topographic variables has not been studied (this is a subject of further work).

Practically, to separate artefacts from actual topographically expressed geological structures and to avoid misinterpretation, one may derive a set of k_h and k_v models from regular DEMs with distinct orientations relative to an irregular DEM. Map patterns indicate actual structures if they can be found on all k_h or k_v maps. Other image patterns may be assumed as artefacts.

Notice finally that the derivation of DTMs from regular DEMs with distinct orientations may be instructive to test possible artificial anisotropy in maps of topographic variables. This can be beneficial for DTM-based geomorphic and geological studies using G, k_h, k_v and R to reveal topographically expressed geological lineaments and faults (Schowengerdt and Glass 1983, Chorowicz *et al.* 1989, Florinsky 1996, 1998b, Collet *et al.* 2000). Since orientation is an essential attribute of these features, a possible false anisotropy in their spatial distribution can lead to misinterpretation. Sometimes, one can reveal near-north-, near-west-, near-northeast-, and near-northwest-striking structures. This anisotropy in map design can be a reflection of the natural anisotropy of topographically expressed geological structures. Indeed, it has been found that a considerable portion of fractured zones, lineaments and faults are marked by near-north, near-west, near-northeast, and near-northwest orientations (Shults 1971, Katterfeld and Charushin 1973, Besprozvanny *et al.* 1994). This phenomenon manifests itself at a wide range of scales, and is observed on the Earth and other terrestrial planets. Topographically expressed lineaments of a tectonic origin are considered in those papers rather than glacial landforms. Reasonable hypotheses of tectonic mechanisms responsible for the lineament orderliness were proposed in papers cited. However, these orthogonal and diagonal linear patterns may also be artefacts caused by geometry of DTM grid, anisotropic errors of DEM compilation, possible anisotropy of DEM interpolation, anisotropy of aliasing artefacts, and possible anisotropy of algorithms for DTM derivation (Florinsky 1993). To separate anisotropic artefacts from actual anisotropic geological structures, one may derive a set of DTMs from regular DEMs with distinct orientations. If anisotropic patterns are found on all maps regardless of DEM orientation, they indicate natural anisotropic structures.

5. Conclusions

This paper presents new interpretations of data processing errors familiar for the DTM community. The errors cause artefacts that can adversely effect DTM-based studies. Explanations of artefact causes and ways to avoid them are carried out in the context of known elements of the theory of signal processing.

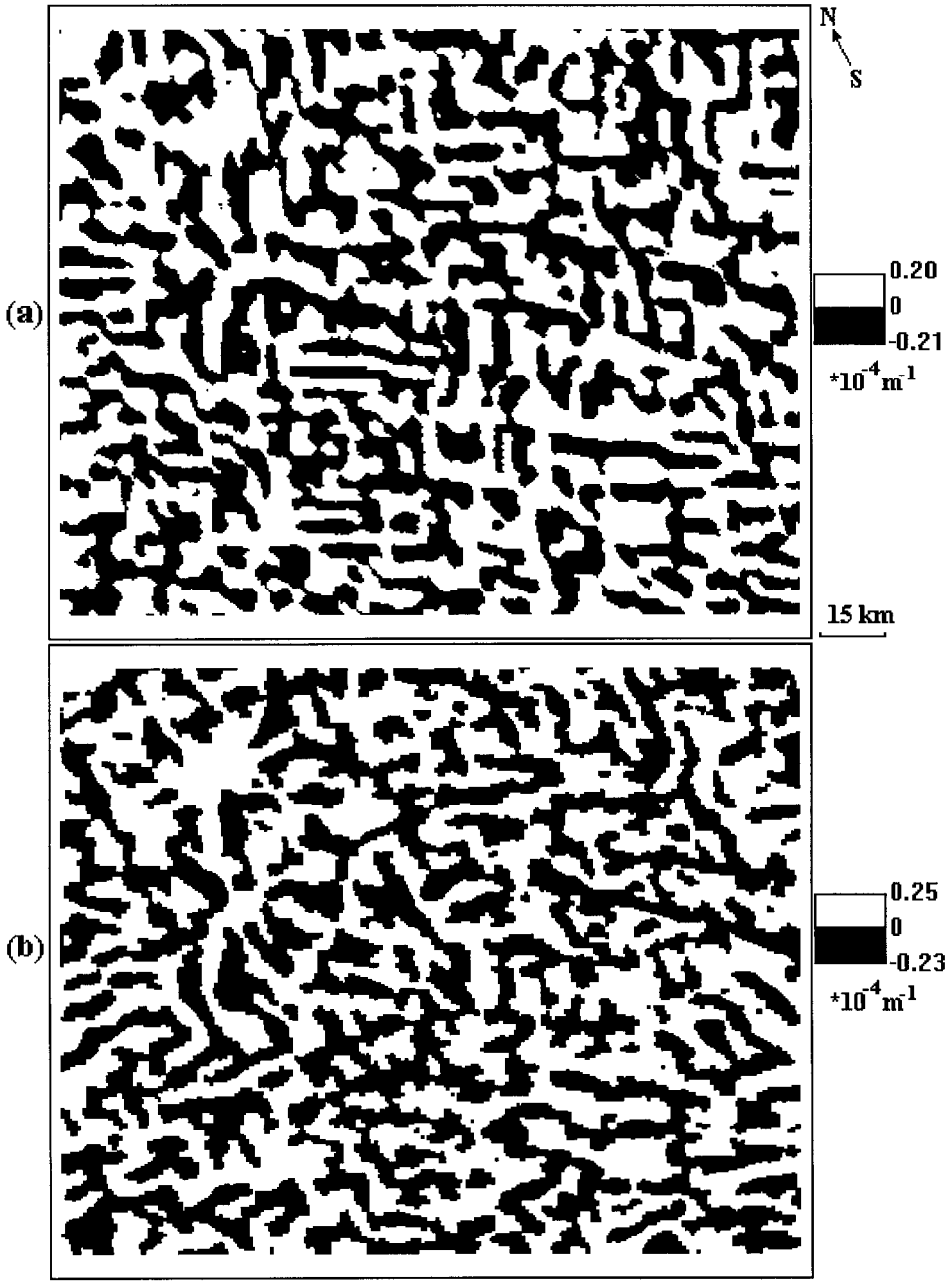

Figure 8. The interstream area of the Kuma and the Kalaus Rivers: k_h maps derived from DEMs with (*a*) 0°-; (*b*) 25°-; (*c*) 90°-rotation of the regular grid.

As Pike (2000) has noted, the discipline of digital terrain modelling is a result of integration of knowledge, principles and methods of earth and computer sciences, mathematics and engineering. The paper presented clearly demonstrates one aspect of the relationship between digital terrain modelling and fields of signal and image

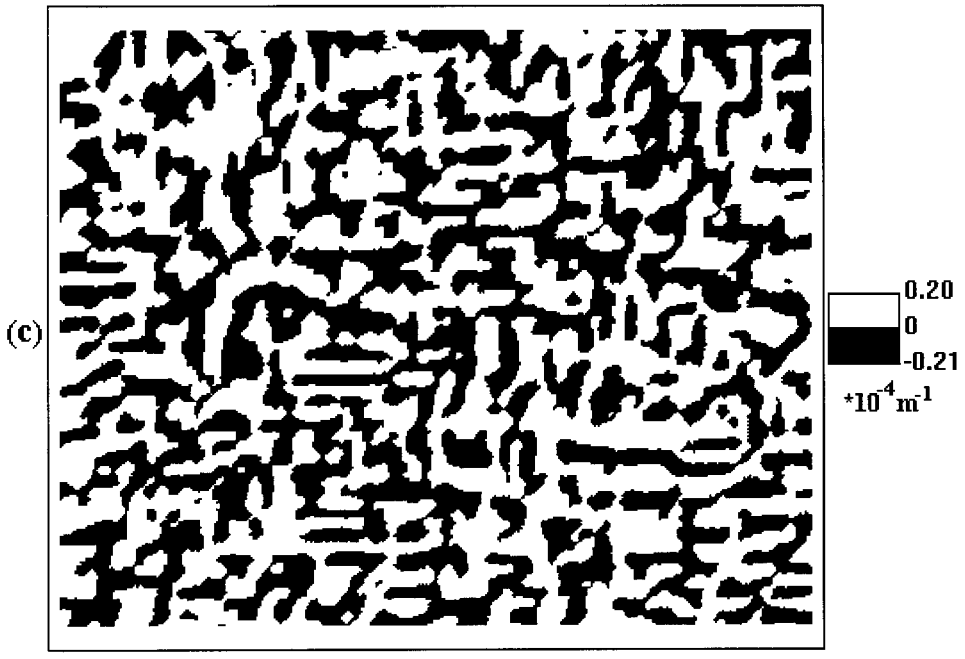

processing. Three error classes discussed are not peculiar for digital terrain modelling only. To avoid these errors successfully, it is essential to understand their actual parents. Broadly speaking, a DTM user should see digital terrain modelling in its association with other fields of the science and engineering.

Methods of digital terrain modelling are scale independent. They are applicable at a broad range of spatial scales (detailed, field, catchment, regional, national, subcontinental and global levels) with equal facility (Pike 2000). Three classes of DEM errors discussed are scale independent too. They can occur at any DEM scale, so knowledge of them is important for all DTM-based works.

In the paper we used ordinary interpolation methods and only visual interpretation of the test results. It might be useful to investigate the artefacts discussed using more sophisticated interpolation techniques and some kind of statistical analysis of DTMs. However, this is a subject of future work.

In the study we used the LandLord package (Florinsky *et al.* 1995) for the Delaunay triangulation with a piecewise smooth interpolation and the weighted average interpolation, calculation and mapping of topographic variables (figures 2, 4–6, 8 and 9). We also used the Surfer (© 1993–96, Golden Software) for the Delaunay triangulation with a linear interpolation (§2.2). The approximation of the square-wave function (figure 1(*b–e*)) was carried out with the Maple V Release 3.0 for Microsoft Windows (© 1981–94, Waterloo Maple Software, University of Waterloo). The illustration of the differentiation of the one-dimensional signal (figure 3) was produced with the Microsoft Excel 97 (© 1985–97, Microsoft).

Acknowledgments

The author is grateful to Dr P. A. Shary (Institute of Physical, Chemical and Biological Problems of Soil Science, Russian Academy of Sciences, Pushchino, Russia)

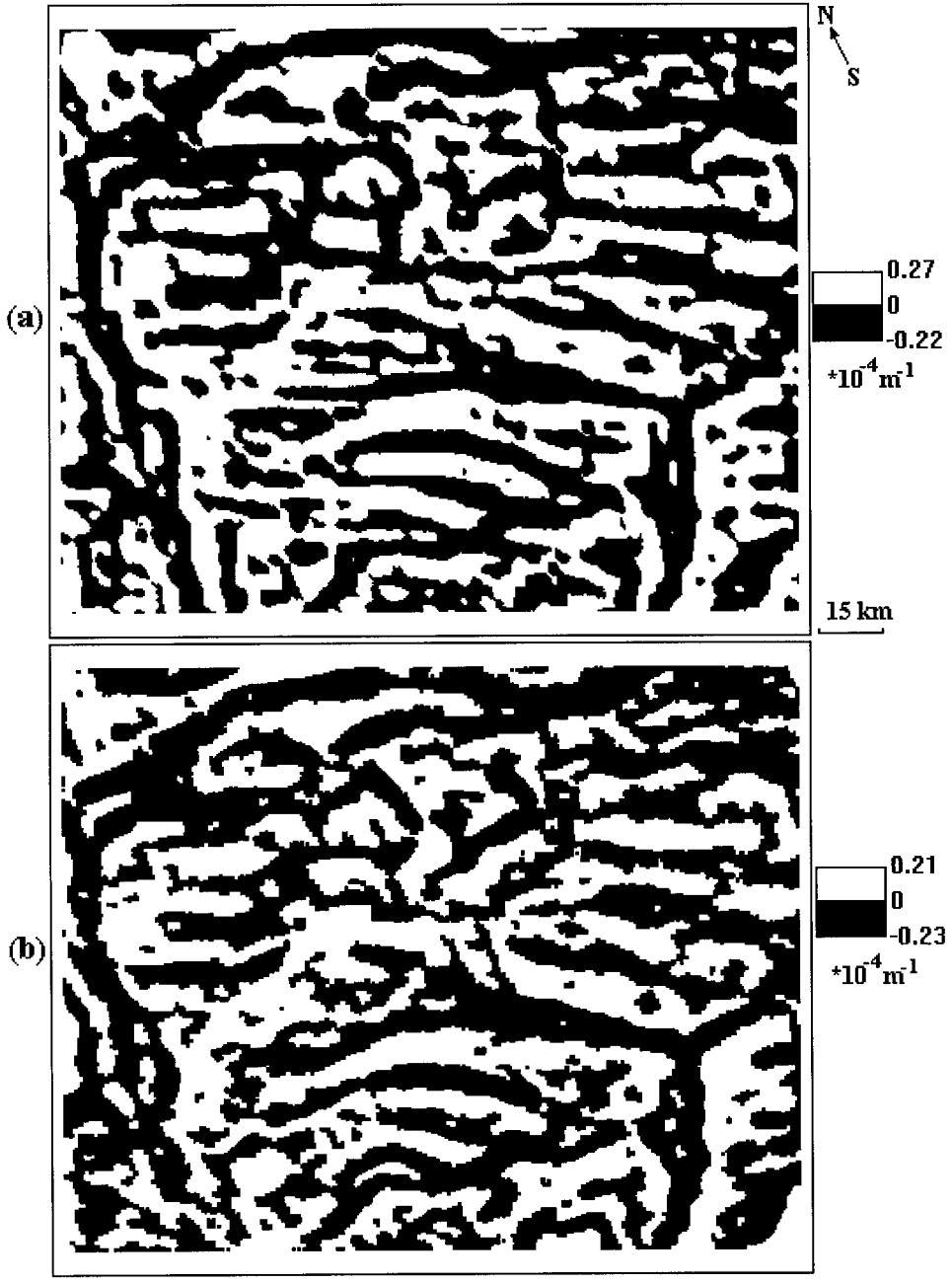

Figure 9. The interstream area of the Kuma and the Kalaus Rivers: k_v maps derived from DEMs with (*a*) 0°-; (*b*) 25°-; (*c*) 90°-rotation of the regular grid.

for fruitful discussions as well as Professor A. M. Molchanov (Institute of Mathematical Problems of Biology, Russian Academy of Sciences, Pushchino, Russia), Professor A. M. Berlyant, Dr S. V. Chistov (Geographical Faculty, Moscow State University, Moscow, Russia) and anonymous referees for useful criticism. The

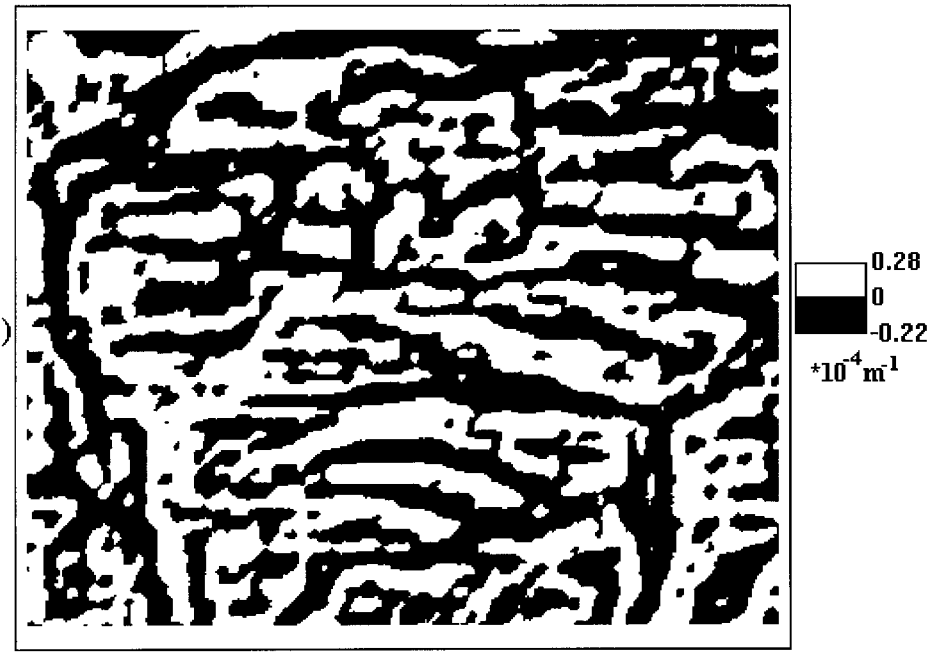

work was carried out with partial support of the NSERC program for Visiting Fellowships in Canadian Government Laboratories.

Appendix. Calculation of local topographic variables

Once elevations are given by $z = f(x, y)$ where x and y are plane Cartesian co-ordinates, local topographic variables are functions of the partial derivatives of z (Shary 1991):

$$G = \arctan\sqrt{p^2 + q^2} \tag{A1}$$

$$A = \arctan\left(\frac{q}{p}\right) \tag{A2}$$

$$k_h = -\frac{q^2 r - 2pqs + p^2 t}{(p^2 + q^2)\sqrt{1 + p^2 + q^2}} \tag{A3}$$

$$k_v = -\frac{p^2 r + 2pqs + q^2 t}{(p^2 + q^2)\sqrt{1 + p^2 + q^2)^3}} \tag{A4}$$

$$H = -\frac{(1 + q^2)r - 2pqs + (1 + p^2)t}{2\sqrt{(1 + p^2 + q^2)^3}} \tag{A5}$$

$$K = \frac{rt - s^2}{(1 + p^2 + q^2)^2} \tag{A6}$$

where

$$r = \frac{\partial^2 z}{\partial x^2},\ t = \frac{\partial^2 z}{\partial y^2},\ s = \frac{\partial^2 z}{\partial x\,\partial y},\ p = \frac{\partial z}{\partial x},\ q = \frac{\partial z}{\partial y} \tag{A7}$$

Reflectance (R) used for hill shading mapping can be calculated by the following formula of the Lambertian model (Horn 1981):

$$R = \frac{1 - p\cos\theta/\tan\psi - q\sin\theta/\tan\psi}{\sqrt{1+p^2+q^2}\sqrt{1+(\cos\theta/\tan\psi)^2+(\sin\theta/\tan\psi)^2}} \tag{A8}$$

where θ and ψ are the solar azimuth and zenith angles, respectively.

r, t, s, p and q can be calculated by the method of Evans (1980): the polynomial

$$z = \frac{rx^2}{2} + \frac{ty^2}{2} + sxy + px + qy + u \tag{A9}$$

is approximated by the least squares method to the 3 by 3 square-spaced altitude submatrix with a grid size of w. Points of the submatrix $(-w, w, z_1)$, $(0, w, z_2)$, (w, w, z_3), $(-w, 0, z_4)$, $(0, 0, z_5)$, $(w, 0, z_6)$, $(-w, -w, z_7)$, $(0, -w, z_8)$ and $(w, -w, z_9)$ are measured plane Cartesian co-ordinates and elevations of the landsurface. As a result, one can estimate values of r, t, s, p and q at the point $(0, 0, z_5)$ by the following finite-difference approximation formulae:

$$r = \frac{z_1 + z_3 + z_4 + z_6 + z_7 + z_9 - 2(z_2 + z_5 + z_8)}{3w^2} \tag{A10}$$

$$t = \frac{z_1 + z_2 + z_3 + z_7 + z_8 + z_9 - 2(z_4 + z_5 + z_6)}{3w^2} \tag{A11}$$

$$s = \frac{z_3 + z_7 - z_1 - z_9}{4w^2} \tag{A12}$$

$$p = \frac{z_3 + z_6 + z_9 - z_1 - z_4 - z_7}{6w} \tag{A13}$$

$$q = \frac{z_1 + z_2 + z_3 - z_7 - z_8 - z_9}{6w} \tag{A14}$$

Moving the 3 by 3 submatrix along a regular DEM, one can calculate values of r, t, s, p and q for all points of the DEM, excepting boundary points.

Definitions, physical interpretations and examples of application of the local topographic attributes can be found in Florinsky (1998a).

References

Akima, H., 1974, A method of bivariate interpolation and smooth surface fitting based on local procedures. *Communications* of the ACM, **17**, 18–20.

Ayeni, O. O., 1982, Optimum sampling for digital terrain models: a trend towards automation. *Photogrammetric Engineering and Remote Sensing*, **48**, 1687–1694.

Baker, K. D., 1982, Basic image processing concepts. In *Digital Signal Processing*, edited by N. B. Jones. (Stevenage: Peter Peregrinus), pp. 287–318.

Bates, P. D., Anderson, M. G., and Horritt, M., 1998, Terrain information in geomorphological models: Stability, resolution and sensitivity. In *Landform Monitoring, Modelling and Analysis*, edited by S. N. Lane, K. S. Richards, and J. H. Chandler (Chichester: John Wiley), pp. 279–309.

Batson, R. M., Edwards, K., and Eliason, E. M., 1975, Computer-generated shaded-relief images. *Journal of Research of the US Geological Survey*, **3**, 401–408.

Benedetto, J., and Ferreira, P. (Editors), 2000, *Modern Sampling Theory: Mathematics and Applications* (Boston: Birkhäuser Boston).

Besprozvanny, P. A., Borodzich, E. V., and Bush, V. A., 1994, Numerical analysis of

ordering relations in the global network of lineaments. *Physics of the Solid Earth*, **30**, 150–159.

Brown, D. G., and Bara, T. J., 1994, Recognition and reduction of systematic error in elevation and derivative surfaces from 7.5-minute DEMs. *Photogrammetric Engineering and Remote Sensing*, **60**, 189–194.

Burrough, P. A., 1986, *Principles of Geographical Information Systems for Land Resources Assessment* (Oxford: Clarendon Press).

Carter, J. R., 1988, Digital representations of topographic surfaces. *Photogrammetric Engineering and Remote Sensing*, **54**, 1577–1580.

Carter, J. R., 1992, The effect of data precision on the calculation of slope and aspect using gridded DEMs. *Cartographica*, **29**, 22–34.

Central Board of Geodesy and Cartography, 1953. Topographic Map, scale 1:300 000. Charts: VI–L–36 (Dzhankoi), VIII–L–36 (Sevastopol), IX–L–36 (Simferopol), V–L–36 (Kherson) (Moscow: Central Board of Geodesy and Cartography) (in Russian).

Central Board of Geodesy and Cartography, 1968, Topographic Map, scale 1:1 000 000. Chart: L–38 (Pyatigorsk) (Moscow: Central Board of Geodesy and Cartography) (in Russian).

Chang, K.-T., and Tsai, B.-W., 1991, The effect of DEM resolution on slope and aspect mapping. *Cartography and Geographical Information Systems*, **18**, 69–77.

Chorowicz, J., Kim, J., Manoussis, S., Rudant, J., Foin, P., and Veillet, I., 1989, A new technique for recognition of geological and geomorphological patterns in digital terrain models. *Remote Sensing of Environment*, **29**, 229–239.

Collet, B., Taud, H., Parrot, J. F., Bonavia, F., and Chorowicz, J., 2000, A new kinematic approach for the Danakil block using a digital elevation model representation. *Tectonophysics*, **316**, 343–357.

Desmet, P. J. J., 1997, Effects of interpolation errors on the analysis of DEMs. *Earth Surface Processes and Landforms*, **22**, 563–580.

Eklundh, L., and Mårtensson, U., 1995, Rapid generation of digital elevation models from topographic maps. *International Journal of Geographical Information Science*, **9**, 329–340.

Endreny, T. A., Wood, E. F., and Lettenmaier, D. P., 2000, Satellite-derived digital elevation model accuracy: Hydrogeomorphological analysis requirements. *Hydrological Processes*, **14**, 1–20.

Evans, I. S., 1980, An integrated system of terrain analysis and slope mapping. *Zeitschrift für Geomorphologie*, **Supplement 36**, 274–295.

Fikhtengolts, G. M., 1966, *A Course in Differential and Integral Calculus*, Vol. 3, 4th edition (Moscow: Nauka) (in Russian).

Florinsky, I. V., 1993, Analysis of Digital Elevation Models for Recognition of Linear Structures of the Landsurface. Ph.D. Thesis. (Pushchino: Institute of Soil Science and Photosynthesis, Russian Academy of Sciences) (unpublished, in Russian).

Florinsky, I. V., 1996, Quantitative topographic method of fault morphology recognition. *Geomorphology*, **16**, 103–119.

Florinsky, I. V., 1998a, Combined analysis of digital terrain models and remotely sensed data in landscape investigations. *Progress in Physical Geography*, **22**, 33–60.

Florinsky, I. V., 1998b, Derivation of topographic variables from a digital elevation model given by a spheroidal trapezoidal grid. *International Journal of Geographical Information Science*, **12**, 829–852.

Florinsky, I. V., and Kuryakova, G. A., 2000, Determination of grid size for digital terrain models in landscape investigations — Exemplified by soil moisture distribution at a micro-scale. *International Journal of Geographical Information Science*, **14**, 815–832.

Florinsky, I. V., Grokhlina, T. I., and Mikhailova, N. L., 1995, Landlord 2.0: The software for analysis and mapping of geometrical characteristics of relief. *Geodesiya i Cartographiya*, **1995–5**, 46–51 (in Russian).

General Headquarters, 1986, *Topographic Map, scale 1:500 000. Chart L–36–G (Simferopol)* (Moscow: General Headquarters) (in Russian).

Giles, P. T., and Franklin, S. E., 1996, Comparison of derivative topographic surfaces of a DEM generated from stereoscopic SPOT images with field measurements. *Photogrammetric Engineering and Remote Sensing*, **62**, 1165–1171.

Gottlieb, D., and Shu, C.-W., 1997, On the Gibbs phenomenon and its resolution. *SIAM Review*, **39**, 644–668.

Grigorenko, A. M., 1998, *Some Problems of the Theory of a Technical Information*. (Moscow: Ubex Press) (in Russian).

Hewitt, E., and Hewitt, R. E., 1980, The Gibbs–Wilbraham phenomenon: An episode in Fourier analysis. *Archive for History of Exact Sciences*, **21**, 129–160.

Horn, B. K. P., 1981, Hill shading and the reflectance map. *Proceedings of the Institute of Electrical and Electronics Engineers*, **69**, 14–47.

Hunter, G. J., and Goodchild, M. F., 1995, Dealing with error in spatial databases: A simple case study. *Photogrammetric Engineering and Remote Sensing*, **61**, 529–537.

Jähne, B., 1991, *Digital Image Processing: Concepts, Algorithms, and Applications* (Berlin: Springer-Verlag).

Jerri, A. J., 1998, *The Gibbs Phenomenon in Fourier Analysis, Splines and Wavelet Approximation* (Boston: Kluwer Academic Publishers).

Katterfeld, G. N., and Charushin, G. V., 1973, General grid systems of planets. *Modern Geology*, **4**, 253–287.

Makarovič, B., 1973, Progressive sampling for digital terrain models. *ITC Journal*, **1973–3**, 397–416.

Makarovič, B., 1976, A digital terrain model system. *ITC Journal*, **1976–1**, 57–83.

Makarovič, B., 1977, Composite sampling for digital terrain models. *ITC Journal*, **1977–3**, 406–433.

Mark, D. M., 1975, Computer analysis of topography: A comparison of terrain storage methods. *Geografiska* Annaler, 57 A, 179–188.

McCullagh, M. J., 1981, Creation of smooth contours over irregularly distributed data using local surface patches. *Geographical Analysis*, **13**, 51–63.

McCullagh, M. J., 1988, Terrain and surface modelling systems: theory and practice. *Photogrammetric Record*, **12**, 747–779.

McCullagh, M. J., 1998, Quality, use and visualisation in terrain modelling. In *Landform Monitoring, Modelling and Analysis*, edited by S. N. Lane, K. S. Richards, and J. H. Chandler (Chichester: John Wiley), pp. 95–117.

Mitàšovà, H., and Mitàš, L., 1993, Interpolation by regularized spline with tension: I. Theory and implementation. *Mathematical Geology*, **25**, 641–655.

Mitra, S. K., 1998, *Digital Signal Processing: A Computer-Based Approach* (New York: McGraw-Hill).

Moore, I. D., Grayson, R. B., and Ladson, A. R., 1991, Digital terrain modelling: A review of hydrological, geomorphological and biological applications. *Hydrological Processes*, **5**, 3–30.

Nielson, G., and Franke, R., 1984, A method for construction of surfaces under tension. *Rocky Mountain Journal of Mathematics*, **14**, 203–221.

Pike, R. J., 2000, Geomorphometry–diversity in quantitative surface analysis. *Progress in Physical Geography*, **24**, 1–20.

Richards, F. B., 1991, A Gibbs phenomenon for spline functions. *Journal of Approximation Theory*, **66**, 334–351.

Robinson, G. J., 1994, The accuracy of digital elevation model derived from digitised contour data. *Photogrammetric Record*, **14**, 805–814.

Rosenfeld, A., and Kak, A. C., 1982, *Digital Picture Processing, Vol. 1 and 2, 2nd Ed.* (New York: Academic Press).

Sasowsky, K. C., Petersen, G. W., and Evans, B. M., 1992, Accuracy of SPOT digital elevation model and derivatives: Utility for Alaska's North Slope. *Photogrammetric Engineering and Remote Sensing*, **58**, 815–824.

Schowengerdt, R. A., and Glass, C. E., 1983, Digitally processed topographic data for regional tectonic evaluations. *Geological Society of America Bulletin*, **94**, 549–556.

Shary, P. A., 1991, The second derivative topographic method. In *The Geometry of the Earth Surface Structures*, edited by I.N. Stepanov (Pushchino: Pushchino Research Centre Press), pp. 30–60 (in Russian).

Shary, P. A., 1995, Land surface in gravity points classification by complete system of curvatures. *Mathematical Geology*, **27**, 373–390.

Shary, P. A., Kuryakova, G. A., and Florinsky, I. V., 1991, On the international experience

of topographic methods employment in landscape researches (a concise review). In *The Geometry of the Earth Surface Structures*, edited by I. N. Stepanov (Pushchino: Pushchino Research Centre Press), pp. 15–29 (in Russian).

SHULTS, S. S., 1971, Planetary fractures and tectonic deformations. *Geotectonics*, **5**, 203–207.

SIROTKIN, M. P., 1961, Toward calculation of topographic volume by approximate integration techniques. *Izvestiya Vysshikh Uchebnyh Zavedeny, Geodesiya i Aerophotosyemka*, **1961–6**, 39–46 (in Russian).

STEFANOVIC, P., RADWAN, M. M., and TEMPFLI, K., 1977, Digital terrain models: Data acquisition, processing and applications. *ITC Journal*, **1977–1**, 61–76.

VEREGIN, H., 1997, The effects of vertical errors in digital elevation models on the determination of flow-path direction. *Cartography and Geographical Information Systems*, **24**, 67–79.

WATSON, D., 1992, *Contouring: A Guide to the Analysis and Display of Spatial Data* (Oxford: Pergamon Press).

WEIBEL, R., and BRÄNDLI, M., 1995, Adaptive methods for the refinement of digital terrain models for geomorphometric applications. *Zeitschrift für Geomorphologie*, **Supplement 101**, 13–30.

WEIBEL, R., and HELLER, M., 1991, Digital terrain modelling. In *Geographical Information Systems: Principles and Applications*, Vol. 1, *Principles*, edited by D. J. Maguire, M. F. Goodchild, and D. Rhind. (Harlow: Longman), pp. 269–297.

WILSON, J. P., SPANGRUD, D. J., NIELSEN, G. A., JACOBSEN, J. S., and TYLER, D. A., 1998, Global positioning system sampling intensity and pattern effects on computed topographic attributes. *Soil Science Society of America Journal*, **62**, 1410–1417.

WISE, S. M., 1998, The effect of GIS interpolation errors on the use of digital elevation models in geomorphology. In *Landform Monitoring, Modelling and Analysis*, edited by S. N. Lane, K. S. Richards, and J. H. Chandler. (Chichester: John Wiley), pp. 139–164.

WISE, S., 2000, Assessing the quality for hydrological applications of digital elevation models derived from contours. *Hydrological Processes*, **14**, 1909–1929.

WOOD, J. D., and FISHER, P. F., 1993, Assessing interpolation accuracy in elevation models. *IEEE Computer Graphics and Applications*, **13**, 48–56.

ZLATOPOLSKY, A. A., 1992, Program LESSA (Lineament Extraction and Stripe Statistical Analysis): Automated linear image features analysis–experimental results. *Computers and Geosciences*, **18**, 1121–1126.